Acta Tropica 271 (2025) 107891

Contents lists available at ScienceDirect

Acta Tropica

journal homepage: www.elsevier.com/locate/actatropica

Histopathological alterations, local hemorrhage and myotoxic effects induced by *Bothrops mattogrossensis* venom and an acidic isolated phospholipase A_2

Micaela de Melo Cordeiro Eulálio [a], Cindy de Oliveira Bariani [b], Alex Augusto Ferreira e Ferreira [a], Andréia Nalva Bernardi de Lima [a], Hallison Mota Santana [a], Mauro Valentino Paloschi [a], Sulamita da Silva Setúbal [a], Larissa Faustina Cruz [a], Ketlei Monteiro Tavares [a], Carolina Pereira da Silva [a], Milena Daniela Souza Silva [a], Charles Nunes Boeno [a], Paula Helena Santa Rita [c], Andreimar Martins Soares [d], Daniela Priscila Marchi Salvador [e], Juliana Pavan Zuliani [a,f,*]

[a] *Laboratory of Cellular Immunology Applied to Health, Oswaldo Cruz Foundation, FIOCRUZ Rondônia, Porto Velho-RO, Brazil*
[b] *Dr. Ary Pinheiro Base Hospital (HB), Porto Velho, Rondônia, Brazil*
[c] *Bioterium of Dom Bosco Catholic University (UCDB), Campo Grande – MS, Brazil*
[d] *Laboratory of Protein Biotechnology and Bioactive Compounds (LABIOPROT), Oswaldo Cruz Foundation, FIOCRUZ Rondônia, Porto Velho-RO, Brazil*
[e] *Toxic Protein Crystallography Laboratory (CPrTox-Lab), Federal University of Paraíba (UFPB), João Pessoa-PB, Brazil*
[f] *Department of Medicine, Federal University of Rondonia (UNIR), Porto Velho-RO, Brazil*

ARTICLE INFO

Keywords:
Bothrops mattogrossensis
PLA_2
Mouse model
Histopathology
Toxicology
Hemorrhagic

ABSTRACT

Snakebite envenomation is a neglected tropical disease with major health impacts in Latin America, where *Bothrops* species are responsible for vast majority of accidents. Among them, *Bothrops mattogrossensis* is epidemiologically relevant due to its wide distribution and clinical involvement in envenomation. This study aimed to characterize the histopathological and biochemical effects of *B. mattogrossensis* venom (*BmV*) and its isolated acidic phospholipase A_2 (BmPLA$_2$-A) in mice. Skeletal muscle, heart, lung, liver, kidney, and spleen were analyzed histologically, while local toxic effects were assessed through hemorrhagic activity and creatine kinase (CK) release. BmPLA$_2$-A induced discrete and non-significant vascular injury, inflammation, and fibrosis in skeletal muscle, along with vascular congestion and hemorrhagic foci in the heart, lungs, and kidneys. However, it did not produce measurable hemorrhagic halos or significant CK elevation, indicating limited hemorrhagic and myotoxic potential. In contrast, crude venom caused more intense and heterogeneous alterations, including extensive vascular ectasia, hemorrhage, pulmonary fibrosis, and pronounced CK elevation, demonstrating strong myotoxic and hemorrhagic activity. BmPLA$_2$-A and *BmV* induced significant hepatic vascular congestion and increased Kupffer-cell activity, with preserved hepatocyte morphology and discrete sinusoidal disorganization. Splenic tissue remained preserved, showing significant vascular congestion only in the venom-treated group. These findings demonstrate that BmPLA$_2$-A contributes to local inflammation and vascular damage but is not the main determinant of systemic hemorrhage or muscle necrosis, which are primarily mediated by other venom components. From a translational perspective, the identification of catalytically active yet non-myotoxic PLA$_2$s such as BmPLA$_2$-A opens avenues for pharmacological exploration, providing potential molecular tools for probing lipid signaling and therapeutic innovation.

* Corresponding author at: Laboratório de Imunologia Celular Aplicada à Saúde – Fundação Oswaldo Cruz Rondonia, Rua da Beira, 7671 - CEP 76812-245 – Porto Velho, RO, Brazil.
E-mail address: juliana.zuliani@fiocruz.br (J.P. Zuliani).

https://doi.org/10.1016/j.actatropica.2025.107891
Received 7 September 2025; Received in revised form 27 October 2025; Accepted 28 October 2025
Available online 30 October 2025

1. Introduction

Snakebite envenomation constitutes a major neglected tropical disease, affecting rural populations in tropical and subtropical regions of Africa, Asia, Oceania, and Latin America (Who, 2019). Globally, it is estimated that 4.5 to 5.4 million snakebite incidents occur annually, leading to 1.8 to 2.7 million cases of envenomation with permanent sequelae and 90,000 to 138,000 deaths (Silva and Isbister, 2020). In South America, Brazil ranks among the countries with the highest incidence of snakebites envenomation, reporting nearly 29,000 cases annually, of which approximately 90 % are attributed to snakes of the *Bothrops* genus (Rodrigues et al., 2023). Within this genus, *Bothrops mattogrossensis*, distributed across Central-West Brazil, Bolivia, Paraguay, Peru, Uruguay and Argentina, represents an epidemiologically relevant species due to its wide geographical range and involvement in human envenomation (Campbell and Lamar, 2004).

Bothrops venoms are complex mixtures of bioactive molecules, primarily proteins such as snake venom metalloproteinases (SVMPs), serine proteases, and phospholipases A_2 (PLA_2s), in addition to L-amino acid oxidases (LAAO), disintegrins, lectins, and other components that act synergistically to disrupt hemostasis, damage tissues, and trigger inflammatory responses (Angulo and Lomonte, 2009; Mackessy, 2021). Among these, PLA_2s (E.C. 3.1.1.4) represent one of the most abundant protein families in viperid venoms. They catalyze the hydrolysis of phospholipids, generating lysophospholipids and arachidonic acid – the latter serving as a substrate for lipid mediators such as prostaglandins and leukotrienes, which amplify the inflammatory response (Khan and Ilies, 2023).

Clinically, *Bothrops* envenomation is characterized by local manifestations, including pain, edema, extensive hemorrhage, and necrosis, which may progress to permanent disabilities such as fibrosis, tissue loss, and amputations (Mamede et al., 2020). Systemic complications, including coagulopathies and acute kidney injury (AKI), contribute substantially to morbidity and mortality (Rodrigues Sgrignolli et al., 2011). Notably, although antivenom therapy effectively neutralizes circulating toxins and prevents systemic effects, it has limited efficacy in reversing local damage, highlighting the need for a deeper understanding of the underlying venom-induced injury (Alangode et al., 2020).

Histopathological investigations have revealed that venom components target multiple organs and tissues, yielding diverse yet interconnected pathological effects. SVMPs are considered the primary hemorrhagic toxins, disrupting vascular basement membranes, degrading extracellular matrix proteins, and inducing vascular ectasia and hemorrhage (Asega et al., 2020; Gutiérrez et al., 2016). PLA_2s, while less potent in inducing hemorrhage, play a central role in promoting myonecrosis, inflammation, and fibrosis, largely through the recruitment of inflammatory cells and deposition of extracellular matrix proteins (Sano-Martins et al. 1997; Zuliani et al., 2023).

Experimental models demonstrate that these toxins affect skeletal muscle, leading to myonecrosis and regenerative fibrosis; the heart, through vascular congestion, edema, and hemorrhagic foci; and the lungs, by inducing alveolar collapse, vascular damage, and chronic inflammatory infiltrates (Khimmaktong et al., 2022; Oliveira Neto et al., 2017; Ángel-Camilo et al., 2024). The liver and kidneys also represent key targets: hepatocellular congestion and Kupffer cell hyperplasia have been reported following envenomation, while the kidneys are highly susceptible to hemorrhage, congestion, and, in severe cases, tubular necrosis, which clinically manifests as acute kidney injury (Sarkar et al., 2021; Sitprija and Sitprija, 2012; Trevisan-Silva at al., 2023).

Despite advances in toxinology, a limited number of studies have rigorously compared the histopathological effects of crude *Bothrops* venoms with those of isolated toxins in multiple organs within the same experimental framework. Such approaches are essential for delineating the contribution of specific venom components to local and systemic pathophysiology and for identifying potential therapeutic targets beyond conventional antivenom.

In this context, the present study aimed to provide a comprehensive histopathological and biochemical assessment of *B. mattogrossensis* venom and its isolated acidic phospholipase A_2 ($BmPLA_2$-A). The effects were investigated in skeletal muscle, heart, lung, liver, kidney, and spleen, alongside systemic markers of toxicity, including hemorrhagic activity and creatine kinase (CK) release. By comparing the pathological outcomes induced by *B. mattogrossensis* venom and by $BmPLA_2$-A, this work seeks to clarify overlapping and distinct mechanisms of tissue injury, contributing to a more refined understanding of *Bothrops* envenomation and its therapeutic challenges.

2. Materials and methods

2.1. *Bothrops mattogrossensis* snake venom

Bothrops mattogrossensis venom was provided by the Bioterium of the Catholic University Dom Bosco (UCDB), Campo Grande, Mato Grosso do Sul, Brazil, and was maintained in refrigerated conditions at the Bank of Amazonian Venoms at the Laboratory of Biotechnology of Proteins and Bioactive Compounds – FIOCRUZ-RO (authorization: SisGen n° AFCAB61 and IBAMA 718.682).

2.2. Isolation of PLA_2 from *B. mattogrossensis* venom

$BmPLA_2$-A was purified from *Bothrops mattogrossensis* venom through a three-step chromatographic procedure: ion-exchange chromatography on a CM-Sepharose column, hydrophobic interaction chromatography on an n-butyl-Sepharose HP column, and reverse-phase chromatography on a C18 column, as previously described by Eulálio et al. (2025).

2.3. Animals

Male Swiss mice (18–22 g) were used in the experiments. Animals were maintained under controlled temperature conditions with free access to food and water until the time of experimentation. All procedures were approved by the Animal Ethics Committee of the Oswaldo Cruz Foundation – Rondônia (protocol no 2022/03) and conducted in accordance with the guidelines of the Brazilian National Council for the Control of Animal Experimentation (CONCEA).

2.4. Histological processing of the gastrocnemius muscle and collected organs

Experimental groups ($n = 3$ per group) were subjected to envenomation with apyrogenic phosphate-buffered saline (PBS), *B. mattogrossensis* venom (5 μg/mL) or $BmPLA_2$-A (50 μg/mL) for 1 h. Following euthanasia, gastrocnemius muscles and selected organs (heart, lung, liver, kidneys, and spleen) were collected and fixed in Carson's formalin for 24 h at room temperature. Samples were processed by standard histological procedures, including graded ethanol dehydration, xylene clearing, and paraffin embedding. Serial sections (5 μm) were prepared using a microtome, mounted on adhesive slides, and stained with hematoxylin and eosin. Permanent mounting was performed, and histological images were acquired using a Nikon Eclipse 80i microscope (Fiocruz-RO Microscopy Platform) and analyzed with NIS-Elements software. Ten random fields per slide were evaluated at 10 × and 20 × magnifications.

2.5. Quantitative histological analysis

Quantitative histological assessments were performed on hematoxylin–eosin-stained sections of the gastrocnemius muscle, heart, lungs, liver, kidneys, and spleen. Images were analyzed with Python-based computational scripts developed in accordance with the HistomicsTK framework (Pourakpour et al., 2025). This open-source toolkit provides

validated algorithms for color normalization, tissue segmentation, and morphometric feature extraction in digital pathology, ensuring reproducibility and quantitative rigor.

For each organ, three biological replicates (three animals per condition) were evaluated, yielding one slide per animal. From each slide, six randomly selected microscopic fields were selected at 10 × and 20 × magnifications. Images were standardized for spatial scale (μm/pixel) and illumination before analysis. Quantitative parameters included nuclear area fraction (%), structural coherence (a.u.), and organ-specific metrics such as fibrosis (%), inflammation (%), vascular congestion (%), hemorrhage (%), septal thickness (a.u.), Kupffer cell density (%), and tubular index (%), depending on the tissue analyzed. Variables expressed as percentages (%) corresponded to proportional tissue areas, whereas parameters given in arbitrary units (a.u.) represented dimensionless morphometric indices (e.g., texture or alignment scores).

Automated segmentation was performed to distinguish principal histological components, including cell nuclei, muscle fibers, vascular structures, and stromal areas. Each component was quantified by pixel-based morphometric and colorimetric analysis using custom Python routines integrated with the HistomicsTK API and OpenCV libraries. Consistent segmentation thresholds were applied across all images, and fields containing <50 % of analyzable tissue or technical artifacts (folds, air bubbles, overstaining) were automatically excluded.

2.6. Hemorrhagic activity assay

Experimental groups ($n = 5$) received intradermal (i.d.) injections of *B. mattogrossensis* venom (50 μg/mL) or BmPLA$_2$-A (50 μg/mL) in the shaved dorsal skin; controls received 50 μL of apyrogenic saline. After 3 h, animals were euthanized, and the skin was removed for analysis. Hemorrhagic halos were photographed, and their areas were quantified using ImageJ software, following calibration with a 5-mm scale. Subsequently, hemorrhagic regions and equivalent control tissues were excised and incubated in Drabkin's solution (8 mL/g tissue, 24 h). Hemoglobin concentration was determined using a chromogenic assay (LabTest kit) in 96-well plates, with absorbance measured at 420 nm on a Synergy HT spectrophotometer (Biotek). Hemoglobin levels (g/dL) were calculated according to Rucavado et al. (2002).

2.7. Assessment of myotoxicity by serum and residual creatine kinase (CK) activity

Experimental groups ($n = 5$) received intradermal injections of *B. mattogrossensis* venom (50 μg/mL), BmPLA$_2$-A (50 μg/mL), or apyrogenic PBS (control). Three hours post-inoculation, blood samples were collected from the retro-orbital plexus, and plasma was separated by centrifugation for CK quantification using a commercial kit (CK-NAC Liquiform, LabTest). Simultaneously, gastrocnemius muscles were collected, mechanically homogenized in PBS using a tissue homogenizer, and centrifuged; the resulting supernatants were used for residual CK determination. Assays were performed in 96-well plates by incubating 5 μL of plasma or muscle supernatant with 250 μL of reagent at 37 °C for 2 min, followed by immediate spectrophotometric reading at 340 nm (Synergy HT, Biotek).

2.8. Statistical analysis

The statistical analysis was performed using GraphPad Prism version 5.0 (GraphPad Software, USA). Data were expressed as mean ± standard error of the meaning (SEM). Differences among experimental groups were evaluated using one-way analysis of variance (ANOVA), followed by Tukey's post hoc test for multiple comparisons.

3. Results

3.1. Histological processing of the gastrocnemius muscle and collected organs

3.1.1. Gastrocnemius muscle

Histopathological and quantitative analyses of the gastrocnemius muscle revealed progressive morphological alterations among the experimental groups (PBS, BmPLA$_2$-A, and *Bothrops mattogrossensis* venom). In the PBS group, skeletal muscle fibers were preserved, exhibiting normal striation and peripheral nuclei, with no significant degenerative changes. Fibroadipose tissue displayed mild chronic inflammation, discrete to moderate vascular ectasia, and an occasional small hemorrhagic focus (Fig. 1, arrows a–c). Quantitatively, nuclear area values remained low and structural coherence was high, indicating preserved tissue organization (Fig. 1A–B).

In the BmPLA$_2$-A group, skeletal muscle exhibited mild chronic inflammation across all sections, accompanied by vascular proliferation and focal fibrosis. Fibroadipose tissue demonstrated mild to moderate inflammation and fibrosis in some areas. Vascular ectasia was discrete to moderate, with moderate hemorrhage in two sections. No alterations were observed in lymph nodes (Fig. 1 arrows d-f). Quantitative analysis did not demonstrate an increase in nuclear area relative to PBS (Fig. 1A). Structural coherence showed a reduction compared with PBS (Fig. 1B), demonstrating disorganization and loss of muscle fiber alignment. Fibrosis exhibited a nonsignificant upward trend within the quantified fields (Fig. 1C), and inflammation remained low, without a marked rise versus PBS (Fig. 1D).

In the *B. mattogrossensis* venom group, histological alterations were more pronounced and heterogeneous. One section demonstrated intense vascular ectasia and extensive hemorrhage in muscle and fibroadipose tissues; another displayed only mild chronic inflammation in fibroadipose tissue; and a third displayed an intermediate pattern, with mild inflammation, vascular proliferation, fibrosis, and moderate hemorrhage (Fig. 1, arrows g-i). Quantitatively, the venom group displayed the highest nuclear area (Fig. 1A), a marked loss of structural coherence consistent with fiber misalignment and tissue disorganization (Fig. 1B), a higher, though nonsignificant, fibrotic trend within the sampled fields (Fig. 1C), and a clear increase in inflammation (Fig. 1D). Overall, the data reveal a treatment-dependent gradient of muscle damage, where structural coherence and tissue integrity progressively deteriorate from PBS to BmPLA$_2$-A and *B. mattogrossensis* venom, accompanied by increasing inflammation and fibrosis, consistent with venom-induced myonecrotic remodeling.

3.1.2. Heart

Histopathological and quantitative analyses of cardiac tissue revealed progressive and condition-dependent morphological alterations among the experimental groups (PBS, BmPLA$_2$-A, and *Bothrops mattogrossensis* venom). In the PBS group, myocardial fibers displayed normal organization and preserved cellular morphology, with only mild alterations such as discrete ventricular hypertrophy and small hemorrhagic foci. Some sections exhibited mild vascular congestion and ectasia, while others showed focal hemorrhage without significant coronary vessel involvement (Fig. 2, arrows a-d). Quantitatively, the nuclear area and structural coherence remained stable and comparable across groups (Fig. 2A-B), confirming the preservation of myocardial fiber alignment and nuclear morphology under control conditions. Congestion values were low, and hemorrhage remained nearly absent (Fig. 2C-D).

In the BmPLA$_2$-A group, histological changes were more frequent and pronounced compared to PBS. All sections presented discrete ventricular hypertrophy associated with vascular ectasia, congestion, and focal edema, as well as variable degrees of subendocardial and intramyocardial hemorrhage (Fig. 2, arrows e-g). Quantitative analyses confirmed these observations, showing no significant differences in

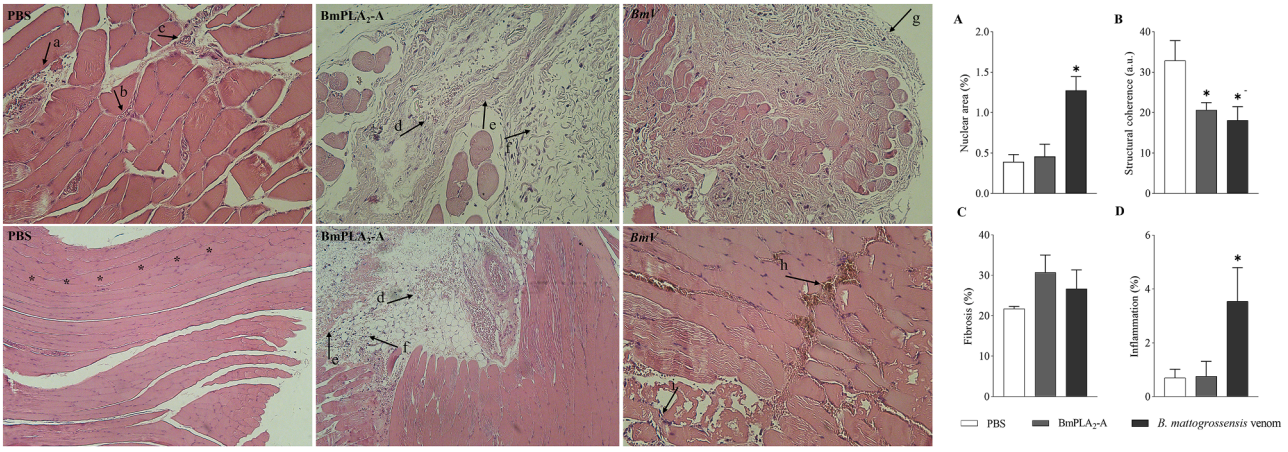

Fig. 1. Histological and quantitative analysis of the gastrocnemius muscle of Swiss mice treated with PBS (control), BmPLA₂-A (50 µg/mL), or *B. mattogrossensis* venom (*BmV*, 5 µg/mL). Representative histological sections (5 µm) stained with hematoxylin and eosin (H&E). In the control (PBS) group, **(a)** a mild nonspecific chronic inflammatory process, **(b)** a small hemorrhagic focus, **(c)** vascular ectasia, and **(*)** skeletal muscle fibers without histopathological alterations were observed. In the BmPLA₂-A-treated group, **(d)** mild hemorrhage, **(e)** focal fibrosis, and **(f)** discrete inflammatory infiltrate were noted. In *BmV* group, **(g)** extensive fibrosis, **(h)** multiple hemorrhagic areas, and **(i)** a marked inflammatory process were observed, indicating severe tissue damage and disorganization. Images were acquired under a Nikon Eclipse 80i microscope at 10 × and 20 × magnifications. Quantitative morphometric analyses (A–D panels) confirmed and complemented the histological findings. **Panel (A)** shows an increased nuclear area in the venom group, reflecting enhanced cellular infiltration. **Panel (B)** demonstrates disorganization and loss of muscle fiber alignment in the toxin and venom groups, indicating reduced structural coherence. **Panel (C)** reveals a trend toward increased fibrosis in both toxin and venom groups, although differences were not statistically significant within the quantified fields. **Panel (D)** indicates a marked increase in inflammation in the venom-treated group compared with PBS and BmPLA₂-A. Bars represent mean ± SD ($n = 3$ animals per group, 6 fields per section), with statistical significance set at $p < 0.05$.

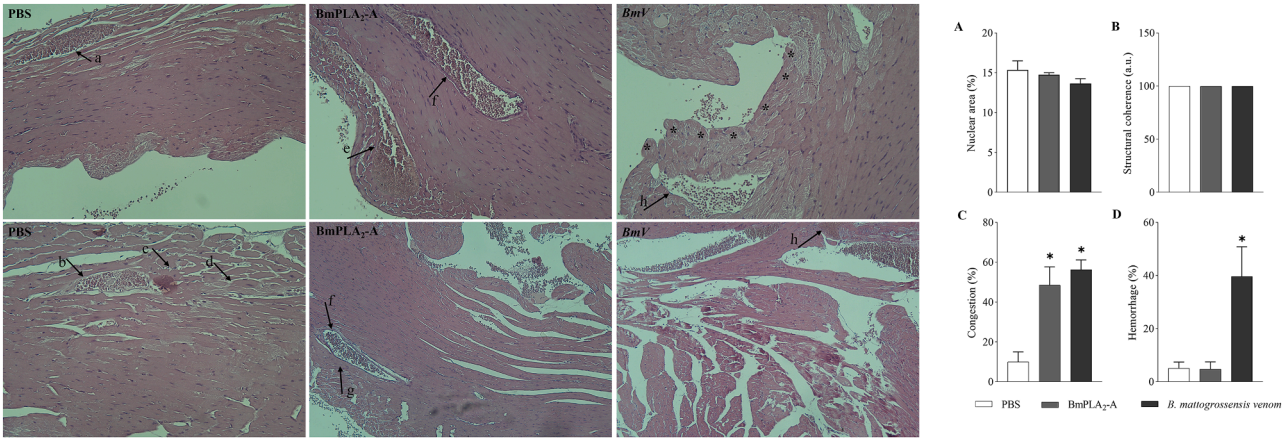

Fig. 2. Histological and quantitative analysis of the heart of Swiss mice treated with PBS (control), BmPLA₂-A (50 µg/mL), or *B. mattogrossensis* venom (*BmV*, 5 µg/mL). Representative histological sections (5 µm) stained with hematoxylin and eosin (H&E). In the PBS group, **(a)** a dilated vessel with a small hemorrhagic focus, **(b)** mild vascular ectasia, **(c)** discrete inflammatory infiltration, and **(d)** mild hypertrophy were observed. In the BmPLA₂-A group, **(e)** hemorrhage, **(f)** vascular ectasia, and **(g)** hypertrophy were identified. In the *BmV* group, **(h)** hemorrhage and **(*)** hypertrophic areas were observed. Images were acquired using a Nikon Eclipse 80i microscope at 10 × and 20 × magnifications. Quantitative morphometric analyses (A–D panels) confirmed and complemented the histological findings. **Panel (A)** shows that nuclear area did not differ significantly among the PBS, BmPLA₂-A, and *BmV* groups. **Panel (B)** demonstrates that structural coherence also remained statistically similar between groups, indicating preserved overall myocardial fiber organization. **Panel (C)** reveals that both the BmPLA₂-A and *BmV* groups exhibited higher vascular congestion compared with PBS, whereas **panel (D)** shows that only the *BmV* group displayed a significant increase in hemorrhage relative to PBS and BmPLA₂-A. Bars represent mean ± SD ($n = 3$ animals per group, 6 fields per section), with statistical significance set at $p < 0.05$.

nuclear area or structural coherence relative to PBS (Fig. 2A-B). However, vascular congestion was markedly increased in the BmPLA₂-A group compared with PBS, reflecting the presence of enlarged and blood-filled vessels (Fig. 2C). Hemorrhage remained low and statistically nonsignificant in this group (Fig. 2D).

Cardiac sections from animals inoculated with *B. mattogrossensis* venom exhibited more intense and heterogeneous tissue alterations than the other groups. Morphological findings included discrete hypertrophy, pronounced vascular congestion and ectasia, edema, and multiple intramyocardial hemorrhagic foci (Fig. 2, arrow h). Quantitative data corroborated these observations, revealing stable nuclear area and coherence values similar to PBS and BmPLA₂-A (Fig. 2A-B), but a significant increase in vascular congestion and a marked rise in hemorrhage compared with both other groups (Fig. 2C-D).

Together, these findings indicate that the toxin (BmPLA₂-A) and whole venom (BmV) induce progressive vascular involvement and tissue injury, characterized primarily by enhanced vascular congestion and intramyocardial hemorrhage. The absence of changes in nuclear area and fiber coherence suggests that early cardiac alterations are predominantly vascular and hemodynamic, preceding overt structural

disorganization of myocardial fibers.

3.1.3. Lung

Histopathological and quantitative analyses of the pulmonary parenchyma revealed progressive, condition-dependent alterations among the PBS, BmPLA₂-A, and *Bothrops mattogrossensis* venom (*BmV*) groups. In the PBS group, only mild changes were observed, including discrete edema, vascular congestion in peribronchial vessels, focal alveolar collapse, vascular ectasia, and mild nonspecific chronic inflammation with occasional granulation tissue deposition. No significant thickening of the alveolar walls was detected (Fig. 3, arrows a-c). Quantitatively, the nuclear area remained low and stable, indicating preserved cellularity and absence of inflammatory infiltration (Fig. 3A). Structural coherence and septal thickness also showed uniform values, consistent with preserved alveolar architecture, while congestion remained minimal (Fig. 3B-D).

In the BmPLA₂-A group, alterations were more frequent and pronounced than in PBS, including alveolar collapse, vascular ectasia, perivascular chronic inflammation, granulation tissue formation, and slight alveolar wall thickening. Certain sections exhibited old hemorrhagic areas with hemosiderophages, while others showed moderate inflammation, congestion, and recent bleeding (Fig. 3, arrows d-g). Quantitatively, a mild but nonsignificant increase in nuclear area was observed, reflecting modest inflammatory recruitment (Fig. 3A). Structural coherence and septal thickness showed a tendency toward reduced alveolar organization and thicker septa, whereas vascular congestion was slightly higher than in PBS (Fig. 3B-D), though without statistical significance.

Lung tissue from the *BmV*-treated animals displayed the most intense and heterogeneous alterations. Morphological findings included alveolar collapse, vascular ectasia, chronic inflammation, granulation tissue deposition, and variable alveolar wall thickening (discrete to moderate). In some sections, moderate inflammation, fibrotic foci, and consistent wall thickening were evident (Fig. 3 arrows h-n). Quantitatively, the venom group exhibited a significant increase in nuclear area compared with PBS (Fig. 3A), consistent with enhanced cellular infiltration and inflammation. Structural coherence remained comparable across groups (Fig. 3B), while vascular congestion and septal thickness showed a trend toward higher values in the BmPLA₂-A and *BmV* groups (Fig. 3C-D), corroborating the morphological evidence of inflammatory and vascular remodeling.

Overall, both BmPLA₂-A and *B. mattogrossensis* venom induced pulmonary alterations more severe than those observed in PBS. Although the general pattern of tissue injury was similar between toxin and venom, the latter promoted greater alveolar wall thickening and a higher nuclear area, suggesting that additional bioactive components in the whole venom potentiate inflammatory and tissue-damaging effects.

3.1.4. Liver

Histological and quantitative analyses of hepatic tissue revealed statistically significant alterations among PBS, BmPLA₂-A, and *Bothrops mattogrossensis* venom (*BmV*) groups. In the PBS group, the hepatic parenchyma was well preserved, with hepatocytes exhibiting granular cytoplasm, round nuclei with dispersed chromatin and prominent nucleoli, and rare binucleated cells without relevant nuclear pleomorphism. Kupffer cells containing dark material were frequent, consistent with normal phagocytic activity, while vascular congestion was mild and hemorrhagic foci were absent (Fig. 4, arrows a-c). Quantitatively, nuclear area and structural coherence remained low and high, respectively, confirming preserved hepatocellular morphology and lobular organization (Fig. 4A-B), while vascular congestion and Kupffer-cell density were the lowest among groups (Fig. 4C-D).

In the BmPLA₂-A group, vascular congestion became more evident, particularly in centrilobular veins and large vessels, occasionally accompanied by discrete microhemorrhages. Hepatocyte morphology remained preserved, without necrotic or degenerative changes. A higher number of Kupffer cells was also detected, suggesting enhanced phagocytic activity in response to the toxin (Fig. 4, arrows d-e). Quantitatively, nuclear area, vascular congestion, and the morphometric proxy for Kupffer-cell density were all significantly higher than in PBS (Fig. 4A, 4C-D), whereas structural coherence was reduced relative to PBS (Fig. 4B), indicating subtle disorganization of hepatocellular cord alignment and sinusoidal architecture despite preserved hepatocyte morphology.

Sections from *BmV*-treated animals revealed a pattern similar to that of the BmPLA₂-A group, with preserved hepatocyte morphology and

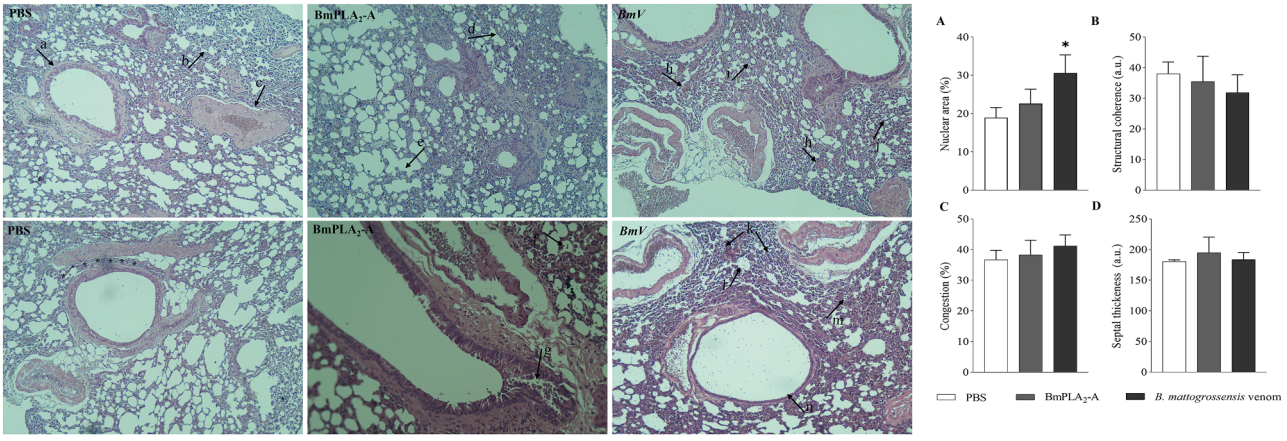

Fig. 3. Histological and quantitative analysis of the lungs of Swiss mice treated with PBS (control), BmPLA₂-A (50 μg/mL), or *B. mattogrossensis* venom (*BmV*, 5 μg/mL). Representative histological sections (5 μm) stained with hematoxylin and eosin (H&E). In the control group (PBS), **(a)** bronchiole, **(b)** collapsed areas, **(c)** arterial wall thickening, and (*) mild inflammatory process are shown. In the BmPLA₂-A group, **(d)** collapsed area, **(e)** alveolar wall thickening, **(f)** alveolar hemorrhage, and **(g)** bronchiolar hemorrhage are observed. In the *BmV*-treated group, **(h)** dilated vessels, **(i)** alveolar thickening, **(j)** mild inflammatory process, **(k)** collapsed alveoli, **(l)** alveolar hemorrhage, **(m)** presence of alveolar macrophages, and **(n)** bronchiolar hemorrhage are identified. Images were obtained under a Nikon Eclipse 80i microscope (10 × and 20 × magnifications). Quantitative morphometric analyses (A–D panels) confirmed and complemented the histological findings. **Panel (A)** shows a significant increase in nuclear area in the venom group, indicating enhanced inflammatory cell infiltration. **Panel (B)** demonstrates that structural coherence remained statistically similar across groups, indicating preserved overall alveolar organization. **Panel (C)** shows a mild, nonsignificant rise in vascular congestion in BmPLA₂-A and *BmV* groups relative to PBS.
Panel (D) reveals a trend toward increased septal thickness in the toxin and venom groups compared with PBS. Bars represent mean ± SD ($n = 3$ animals per group, 6 fields per section), with statistical significance set at $p < 0.05$.

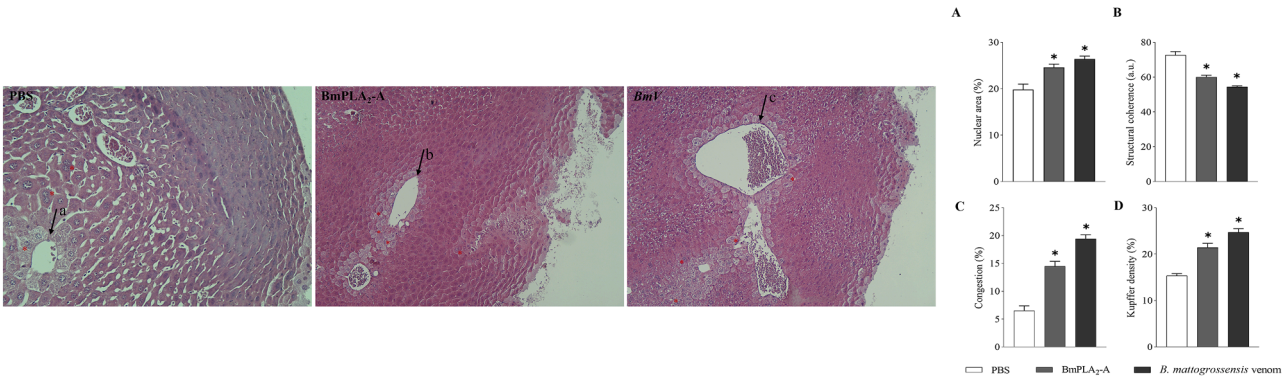

Fig. 4. Histological and quantitative analysis of the liver of Swiss mice treated with PBS (control), BmPLA₂-A (50 µg/mL), or *B. mattogrossensis* venom (*BmV*, 5 µg/mL). Representative histological sections (5 µm) stained with hematoxylin and eosin (H&E). In all experimental groups, centrilobular vein with ballooned cells **(a-c)** and presence of rare binucleated cells **(*)** were observed. Images were obtained using a Nikon Eclipse 80i microscope at 10 × and 20 × magnifications. Quantitative morphometric analyses (A–D panels) confirmed and complemented the histological findings. **Panel (A)** shows an increase in nuclear area in the BmPLA₂-A and BmV groups, reflecting enhanced cellular infiltration and Kupffer-cell activation. **Panel (B)** shows a reduction in structural coherence in the treated groups, indicating mild disorganization of hepatocellular cords and sinusoidal alignment. **Panel (C)** shows an increase in vascular congestion in both treated groups, particularly marked in the BmV group, reflecting enhanced vascular dilation and blood pooling. **Panel (D)** shows an increase in the morphometric proxy for Kupffer-cell density in the treated groups, indicating intensified phagocytic activity. Bars represent mean ± SD ($n = 3$ animals per group, 6 fields per section), with statistical significance set at $p < 0.05$.

occasional binucleated cells. Discrete microvesiculation, predominantly in centrilobular regions (zone III), suggested early autolytic processes. Congestion in centrilobular veins was more marked, accompanied by rare microhemorrhages and abundant Kupffer cells with pigmented material (Fig. 4, arrows f-g). Quantitatively, the venom group exhibited the highest nuclear area, vascular congestion, and the morphometric proxy for Kupffer cell density, each of which was significantly greater than in the PBS group (Fig. 4A, 4C-D). Structural coherence was significantly reduced relative to PBS group (Fig. 4B), indicating disorganization of hepatocellular cord alignment and sinusoidal architecture. Taken together, the morphometric data demonstrate significant, condition-dependent hepatic alterations rather than subtle tendencies.

3.1.5. *Kidneys*

Histopathological and quantitative analyses of renal tissue revealed distinct patterns of lesion among the PBS, BmPLA₂-A, and *Bothrops mattogrossensis* venom (*BmV*) groups, with a progressive intensification of vascular and parenchymal lesions (Fig. 5, arrows a-c). In the PBS group, the renal parenchyma was largely preserved. Glomeruli appeared small with reduced Bowman's space, proximal tubules exhibited only mild surgical stress, and distal tubules and Henle's loops were unaltered. Occasional vascular ectasia and rare microhemorrhages were noted, with moderate hemorrhage in a single section (Fig. 5, arrow a). Quantitatively, the PBS group showed low nuclear area and high structural coherence values (Fig. 5A-B), consistent with preserved cellular morphology and organized tubular architecture. The tubular index was also the highest among groups, confirming the maintenance of epithelial integrity and luminal definition (Fig. 5C).

In the BmPLA₂-A group, alterations were predominantly vascular, including pronounced ectasia, discrete to moderate congestion, and

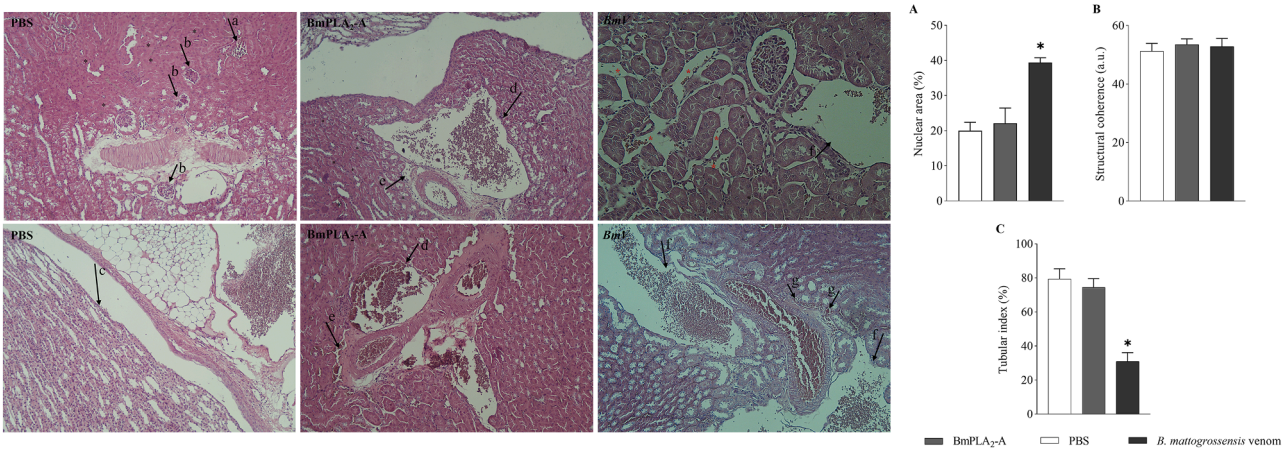

Fig. 5. Histological and quantitative analysis of the kidneys of Swiss mice treated with PBS (control), BmPLA₂-A (50 µg/mL), or *B. mattogrossensis* venom (*BmV*, 5 µg/mL). Representative histological sections (5 µm) stained with hematoxylin and eosin (H&E). In the control group, **(a)** vascular ectasia, **(b)** small glomeruli with reduced Bowman's space, **(c)** narrow Henle's loops without accumulations, and **(*)** proximal tubules showing mild surgical stress were observed. In the BmPLA₂-A group, **(d)** marked vascular ectasia, **(e)** focal hemorrhage, and (*) proximal tubules with mild surgical stress were identified. In the *BmV* group, **(f)** vascular ectasia, (g, *) diffuse hemorrhagic areas, and (*) proximal tubules with signs of surgical stress were observed. Images were obtained using a Nikon Eclipse 80i microscope at 10 × and 20 × magnifications. Quantitative morphometric analyses (panels A–C) confirmed and complemented the histological findings. **Panel (A)** shows a significant increase in nuclear area in the BmV group compared with PBS and BmPLA₂-A, indicating enhanced cellular activation and nuclear hypertrophy. **Panel (B)** shows that structural coherence remained similar across all groups, confirming that global renal architecture was preserved despite vascular alterations. **Panel (C)** shows a marked reduction in the tubular index in the BmV group, reflecting epithelial flattening, luminal dilation, and tubular disorganization. Bars represent mean ± SD ($n = 3$ animals per group, 6 fields per section), with statistical significance set at $p < 0.05$.

focal hemorrhages in small- and medium-caliber vessels (Fig. 5, arrow b). Glomerular and tubular morphology remained largely comparable to PBS. Quantitatively, nuclear area did not differ from PBS (Fig. 5A); structural coherence was unchanged relative to PBS (Fig. 5B), indicating maintenance of global tissue organization; and the tubular index showed a slight, non-significant downward trend (Fig. 5C), compatible with subtle epithelial flattening without overt structural failure.

The *BmV* group exhibited the most pronounced lesions, characterized by intense vascular ectasia, diffuse parenchymal hemorrhage, and areas of tubular disarray, while glomeruli remained structurally recognizable (Fig. 5, arrow c). Quantitatively, the nuclear area was markedly and significantly elevated compared with PBS (Fig. 5A). Structural coherence remained comparable across groups (Fig. 5B), indicating that the venom's predominant quantitative signature was not a loss of global coherence but rather a shift in nuclear metrics and tubular integrity. Consistent with this, the tubular index was significantly reduced only in the venom group (vs. PBS group), whereas BmPLA₂-A showed only a non-significant tendency to decrease (Fig. 5C), supporting substantial epithelial compromise specifically under whole-venom exposure.

3.1.6. Spleen

Histopathological and quantitative analyses of the spleen revealed overall preserved parenchymal organization across all experimental groups (PBS, BmPLA₂-A, and *Bothrops mattogrossensis* venom), with maintained distinction between white and red pulp compartments. The white pulp consisted of homogeneous lymphoid aggregates predominantly composed of small lymphocytes and rare macrophages, while the red pulp exhibited dilated sinusoids rich in erythrocytes.

In the PBS group, tissue sections demonstrated a homogeneous pattern with occasional thin fibrous septa, discrete vascular proliferation, and focal vascular congestion (Fig. 6, arrow a). Quantitatively, nuclear area values were low and structural coherence remained high, consistent with an intact and organized parenchyma (Fig. 6A-B).

The BmPLA₂-A group presented similar findings, with discrete vascular congestion in the red pulp, rare fibrous septa, and dilated sinusoids containing abundant erythrocytes (Fig. 6, arrow b). Quantitative analysis revealed no significant change in nuclear area compared with PBS, and structural coherence remained stable, indicating preserved microarchitectural organization (Fig. 6A-B). Congestion levels were slightly elevated but remained low overall (Fig. 6C).

In the *B. mattogrossensis* venom group, vascular alterations were consistently more evident, with marked sinusoidal dilation and diffuse erythrocyte accumulation throughout the red pulp (Fig. 6, arrow c). Quantitatively, nuclear area and structural coherence remained comparable to PBS and BmPLA₂-A (Fig. 6A-B), indicating preserved cellular organization and tissue integrity. In contrast, vascular congestion showed a statistically significant increase relative to both PBS and BmPLA₂-A (Fig. 6C), confirming the morphologically evident enhancement of splenic vascular engorgement in the venom-treated animals.

3.2. Evaluation of the hemorrhagic process

Fig. 7 illustrates the qualitative and quantitative assessment of hemorrhagic halos induced by intradermal inoculation of *B. mattogrossensis* venom and $BmPLA_2$-A in Swiss mice. In the photographic images (Fig. 7A), no hemorrhagic halos were observed in the control group (saline), whereas animals inoculated with *B. mattogrossensis* venom (50 μg/mL) exhibited evident halos with intense coloration and extensive hemorrhage, confirming the venom's hemorrhagic activity. In contrast, $BmPLA_2$-A (50 μg/mL) did not induce visible hemorrhagic halos, indicating an absence of hemorrhagic activity.

Quantitative analysis (Fig. 7B) revealed that only the venom group displayed a statistically significant enlargement in hemorrhagic area compared to the control. Measurements in the $BmPLA_2$-A group did not differ significantly from control, supporting the absence of a measurable hemorrhagic effect.

Hemoglobin quantification within hemorrhagic halos further corroborated these findings. Venom-inoculated animals demonstrated significantly elevated hemoglobin levels compared with controls, while $BmPLA_2$-A values remained similar to those of the control group.

Collectively, these results demonstrate that *B. mattogrossensis* venom exerts a potent hemorrhagic effect, whereas $BmPLA_2$-A lacks significant hemorrhagic activity. This suggests that other venom components, probably metalloproteinases, play a central role in hemorrhage induction.

3.3. Myotoxic effect

In the control group (PBS), serum and residual creatine kinase (CK) levels remained close to baseline values (Fig. 8), indicating the absence of significant muscle damage. In contrast, animals inoculated with *B. mattogrossensis* venom (50 μg/mL) displayed a pronounced elevation in serum CK, consistent with acute and severe myotoxicity. Conversely, the $BmPLA_2$-A group (50 μg/mL) did not show a significant elevation in serum or residual CK compared with PBS, suggesting minimal or absent myotoxic activity. These findings indicate that venom contains components responsible for pronounced muscle damage, whereas isolated $BmPLA_2$-A exerts minimal to undetectable myotoxic effect.

4. Discussion

The present study provides a comprehensive histopathological and biochemical evaluation of the effects of *Bothrops mattogrossensis* venom and its isolated phospholipase A_2 ($BmPLA_2$-A) on multiple organs and

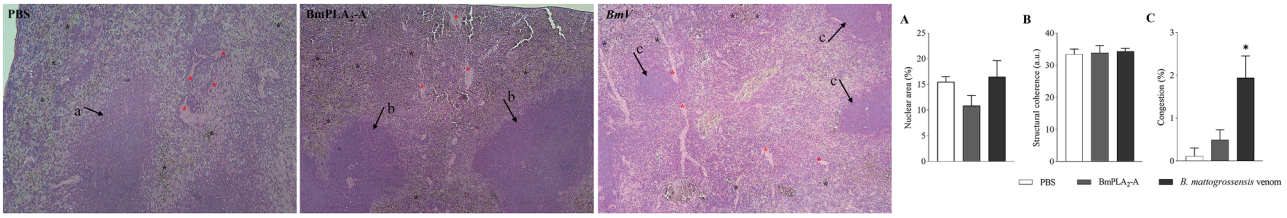

Fig. 6. Histological and quantitative analysis of the spleen of Swiss mice treated with PBS (control), BmPLA₂-A (50 μg/mL), or *B. mattogrossensis* venom (*BmV*, 5 μg/mL). Representative histological sections (5 μm) stained with hematoxylin and eosin (H&E). In all experimental groups, representative sections show well-preserved parenchymal architecture with distinct white pulp **(a-c)** and red pulp **(*)** containing dilated sinusoids filled with erythrocytes and occasional thin fibrous septa **(*)**. Images were obtained using a Nikon Eclipse 80i microscope at 10 × and 20 × magnifications. Quantitative morphometric analyses (A–C panels) corroborated the histological findings. **Panel (A)** shows that the nuclear area remained comparable among groups, indicating preserved cellular density. **Panel (B)** shows stable structural coherence across treatments, consistent with maintenance of splenic microarchitecture. **Panel (C)** demonstrates a significant increase in vascular congestion in the venom group compared with PBS and BmPLA₂-A, reflecting enhanced vascular engorgement within the red pulp. Bars represent mean ± SD ($n = 3$ animals per group, 6 fields per section), with statistical significance set at $p < 0.05$.

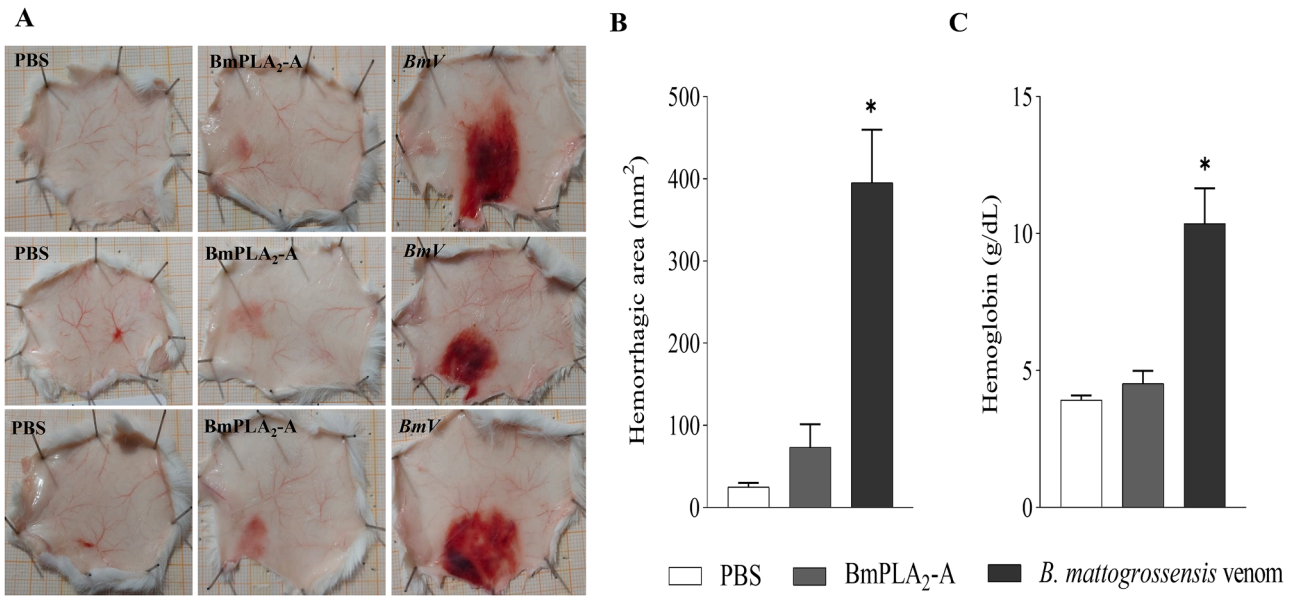

Fig. 7. Evaluation of the hemorrhagic effect induced by *B. mattogrossensis* venom and the BmPLA₂-A toxin compared with the control group (PBS). (A) Representative images of hemorrhagic halos under different experimental conditions, obtained 3 h after intradermal inoculation. **(B)** Quantification of hemorrhagic area (mm^2) using ImageJ software. **(C)** Hemoglobin concentration (g/dL) in hemorrhagic tissues, determined by the Drabkin method. Data are expressed as mean ± standard deviation, with statistical significance set at $p < 0.05$.

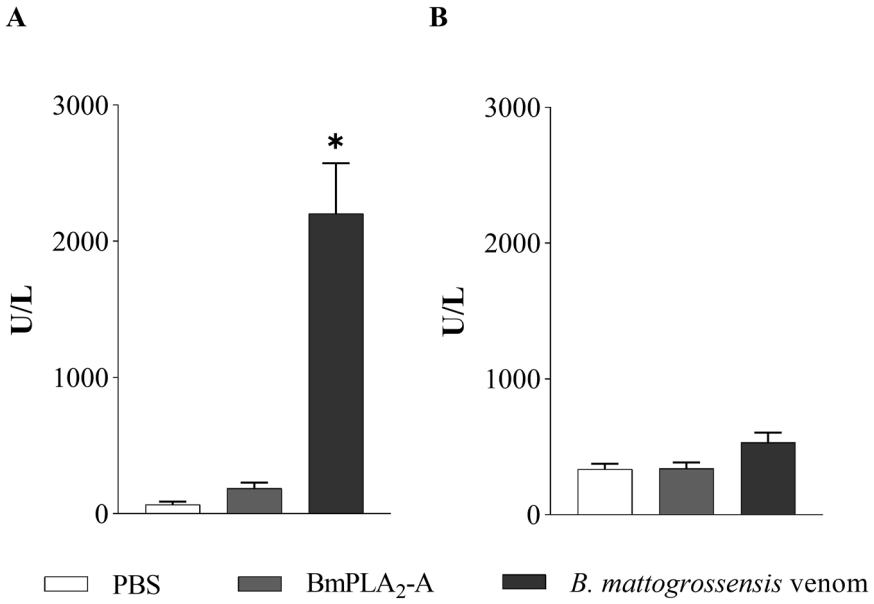

Fig. 8. Evaluation of myotoxic activity by creatine kinase (CK) measurement. (A) Serum CK levels and **(B)** residual CK levels in animals inoculated with saline solution (PBS), BmPLA₂-A (50 μg/mL) or *B. mattogrossensis* venom (50 μg/mL). Data are expressed as mean ± standard deviation, with statistical significance set at $p < 0.05$.

tissues, including skeletal muscle, heart, lung, liver, kidney, and spleen, as well as on systemic parameters such as hemorrhage and creatine kinase (CK) activity. Together, the findings highlight both overlapping and distinct pathological outcomes elicited by *B. mattogrossensis* venom compared with the BmPLA₂-A, underscoring the complexity of the venom's pathophysiological mechanisms and the contribution of specific components.

The assessment of the biological effects of *B. mattogrossensis* venom and the isolated BmPLA₂-A using an animal model revealed histological findings that expand the understanding of tissue damage associated with *Bothrops* envenomation. In muscle and fibroadipose tissues, the analyses demonstrated extensive hemorrhage, chronic inflammation, vascular proliferation, and fibrosis, confirming myotoxicity as a major pathological effect of the venom.

In contrast, animals injected with BmPLA₂-A presented more homogeneous and less severe changes, characterized by discrete chronic inflammation and mild vascular proliferation, without significant increase in nuclear area or evidence of necrosis. These findings indicate that BmPLA₂-A elicits subtle inflammatory and fibrotic responses without overt myonecrotic activity, reinforcing its limited cytotoxic potential and suggesting that the observed alterations are subclinical and reversible rather than degenerative

The most pronounced vascular ectasia and hemorrhagic foci were observed in the group inoculated with *B. mattogrossensis* venom,

highlighting the synergistic action of its components, particularly metalloproteinases. These enzymes degrade extracellular matrix components, disrupt vascular integrity, and promote hemorrhage (Asega et al., 2020; Gutiérrez et al., 2016). In contrast, animals injected with BmPLA₂-A presented more homogeneous and less severe changes, characterized by mild to moderate chronic inflammation, vascular proliferation, and fibrosis. These findings support the role of PLA₂s in promoting local inflammation and tissue remodeling, processes commonly linked to extracellular matrix deposition and fibrosis development (Sano-Martins et al., 1997).

The vascular ectasia and hemorrhagic foci observed with *B. mattogrossensis* venom further corroborate the potentiation of tissue damage by the synergistic interaction of multiple toxins (Amaral et al., 1986). This synergism was also evident in renal lesions, in which vascular ectasia and hemorrhage are largely attributed to SVMPs (Sitprija and Sitprija, 2012). By contrast, the group inoculated with BmPLA₂-A displayed only moderate vascular alterations, such as congestion and ectasia, without significant evidence of acute tubular necrosis or a strong inflammatory response. The absence of tubular necrosis, however, does not exclude early functional impairment, since renal injury following envenomation often begins with hemodynamic and microvascular disturbances that precede overt structural damage.

Although previous studies describe PLA₂-induced inflammation and tubular necrosis (Mittal, 1994; Marinho et al., 2021), the present findings suggest that BmPLA₂-A alone exerts a milder toxic effect on renal parenchyma compared to venom. This effect is likely attributable to the acidic profile of BmPLA₂-A, since acidic Asp-49 PLA₂s generally present lower cytotoxicity and inflammatory potential than their basic counterparts.

Acute kidney injury (AKI) is a severe complication of *Bothrops* envenomation, clinically characterized by oliguria and increased serum creatinine, potentially progressing to severe renal dysfunction requiring dialysis (Rodrigues Sgrignolli et al., 2011). Epidemiological studies report a highly variable prevalence of AKI (1.4 %–38 %), depending on species, envenomation severity, and patient-related factors. AKI is recognized as the leading cause of mortality among patients who survive the initial systemic effects of the venom, with mortality rates reaching up to 19 % (Rodrigues Sgrignolli et al., 2011; Meena et al., 2024; Otero-Patiño, 2009).

The pathophysiology of *Bothrops*-induced AKI is multifactorial, combining direct cytotoxicity of venom toxins with systemic hemodynamic disturbances such as hypotension and hypovolemic shock, as well as rhabdomyolysis and hemolysis leading to myoglobinuria, hemoglobinuria, and glomerular microthrombi deposition (Sitprija and Sitprija, 2012; Marinho et al., 2021). Experimental evidence indicates that *Bothrops* venom components can be detected in renal parenchyma as early as 30 min after intravenous injection in animal models, with elimination observed in urine within 3 h (Mello et al., 2010). These findings support the present results, which demonstrate an early interaction of *B. mattogrossensis* venom with renal structures, evidenced by histopathological changes as soon as 1 h after experimental envenomation.

Histological analysis of cardiac muscle under different experimental conditions revealed distinct morphological alterations, indicating variable degrees of tissue damage in response to BmPLA₂-A and *B. mattogrossensis* venom. Compared to the PBS control group, both toxin-treated groups exhibited more pronounced histological changes, particularly vascular congestion and hemorrhagic foci.

Within the PBS group, only mild alterations were observed, including slight hypertrophy and sparse hemorrhagic areas. These findings are consistent with previous reports indicating that saline administration does not induce significant cardiac histopathological changes, as described by Khimmaktong et al. (2022), who reported that mice inoculated with PBS did not present cardiac lesions.

Animals inoculated with BmPLA₂-A exhibited marked alterations, including ventricular hypertrophy, vascular congestion, edema, and subendocardial and intramyocardial hemorrhages. These results are consistent with the cardiotoxic effects of PLA₂s previously described in the literature. PLA₂s have been show to directly damage cardiomyocytes and the vasculature, leading to microvascular dysfunction and erythrocytes extravasation into the interstitium (Khimmaktong et al., 2022; Ángel-Camilo et al., 2024). The edema observed in this group is attributable to the inflammatory response induced by the toxin, which enhances vascular permeability and promotes fluid accumulation in the interstitial space (Sampat et al., 2023).

Although the general pattern of lesions resembled those observed with BmPLA₂-A, the intensity and extent of vascular injury were markedly greater in the *B. mattogrossensis* venom group. This enhanced effect is likely related to the synergistic action of proteolytic venom components, particularly metalloproteinases, which exert potent hemorrhagic activity (Baldo et al., 2010; Madrigal et al., 2012). The presence of extensive subendocardial and intramyocardial hemorrhages supports the capacity of *B. mattogrossensis* venom to cause severe vascular injury, probably through extracellular matrix degradation and disruption of vascular wall integrity.

Moreover, the vascular congestion, ectasia, and hemorrhages observed in both BmPLA₂-A and *B. mattogrossensis* venom groups resemble the cardiac effects reported for other snake venoms from the Elapidae and Viperidae families. Khimmaktong et al. (2022), demonstrated that *Calloselasma rhodostoma* venom induced cardiac fiber hypertrophy, vascular congestion, and macrophage infiltration, indicative of inflammation and vascular damage comparable to the present findings. Similarly, Ángel-Camilo et al. (2024), reported interfibrillar edema and cardiocytolysis in experimental models exposed to *Lachesis acrochorda* venom, further supporting the capacity of snake venoms to induce severe cardiac tissue injury.

The histopathological analysis of lung parenchyma in animals treated with BmPLA₂-A and *B. mattogrossensis* venom revealed significant alterations, some of which resemble pulmonary effects previously reported for other snake venoms, such as *Crotalus durissus cascavella* and *Crotalus durissus terrificus*. The changes observed, alveolar collapse, vascular ectasia, hemorrhage, and inflammatory processes, are partially consistent with previous findings of Oliveira et al. (2017), who described atelectasis, mild emphysema, and pulmonary edema in animals exposed to *C. d. cascavella* venom. Both studies highlight the ability of snake venoms to damage lung tissue, compromising its structure and function.

However, notable differences were also identified. In the present study, alveolar wall thickening and nonspecific chronic inflammation were observed, features not reported by Oliveira et al. (2017). Although trends toward septal thickening and vascular congestion were observed in the BmPLA₂-A and venom groups, these did not reach statistical significance, indicating early subacute remodeling rather than severe inflammatory injury.

These discrepancies suggest that each venom triggers distinct tissue responses, likely due to differences in toxin composition and mechanisms of action. While *C. d. cascavella* venom appears to induce predominantly acute changes, such as edema and emphysema. *B. mattogrossensis* venom promotes a more chronic response, with a tendency toward fibrosis and alveolar thickening. Such variation underscores the complexity of snake venom pathology and the need for species-specific investigations.

The alveolar collapse and vascular ectasia observed in both BmPLA₂-A and *B. mattogrossensis* venom groups may be associated to alterations in pulmonary mechanics. Oliveira et al. (2017), similarly reported moderate atelectasis, discrete emphysema, and edema in animals exposed to *C. d. cascavella*, suggesting that pulmonary ventilation can be compromised by inflammatory and obstructive processes, leading to increased mechanical heterogeneity of the lungs. The pulmonary hemorrhage observed in this study mirrors the hemorrhagic effects reported for *C. d. cascavella* venom, which has been attributed to PLA₂ and crotamine, components recognized for their myotoxic and pro-inflammatory properties (Nonaka et al., 2008).

The inflammatory infiltrate observed in animals inoculated with BmPLA₂-A and crude venom is consistent with the lymphocytic and plasmacytic infiltration described by Oliveira et al. (2017), in response to *C. d. cascavella* venom. This effect is likely related to chemotaxis mediated by arachidonic acid metabolites (prostaglandins, leukotrienes, and lipoxins), which recruit inflammatory cells to the site of injury (Triggiani et al., 2006). The greater intensity of inflammation in the *B. mattogrossensis* venom group suggests an additional contribution from bioactive components such as SVMPs, which may exacerbate the inflammatory response and potentiate tissue injury.

Hepatic alterations following exposure to *B. mattogrossensis* venom and its acidic phospholipase A₂ (BmPLA₂-A) were mild to moderate but statistically significant compared with the PBS control. The main histopathological features included marked vascular congestion, particularly in centrilobular veins, discrete microhemorrhages, and increased Kupffer-cell density, while hepatocyte morphology remained largely preserved. Quantitative analyses confirmed significant increases in nuclear area, vascular congestion, and Kupffer-cell density in both the BmPLA₂-A and *BmV* groups compared with PBS controls, accompanied by a reduction in structural coherence, indicating subtle to moderate disruption of lobular organization and sinusoidal alignment rather than extensive parenchymal necrosis.

These findings indicate that hepatic response to envenomation is statistically significant but morphologically mild, consistent with an early, sublethal phase of microcirculatory disturbance and Kupffer-cell activation. The elevated Kupffer-cell index reflects enhanced phagocytic and detoxifying activity in response to circulating venom components, whereas the reduction in structural coherence suggests subtle disorganization of lobular architecture rather than hepatocellular necrosis. Similar early hepatic responses have been reported in response to venoms of *Calloselasma rhodostoma, Naja haje*, and *Crotalus durissus terrificus*, which induce Kupffer-cell hyperplasia, sinusoidal congestion, and vascular dilation preceding necrotic or degenerative changes at later time points (Khimmaktong et al., 2022; Barraviera and Pereira, 1995).

The absence of overt necrosis or marked nuclear pleomorphism in the present study likely reflects the short post-exposure interval (1 h), insufficient to trigger irreversible cytotoxicity. Nonetheless, the morphometric evidence of architectural disorganization and increased Kupffer-cell activity supports the hypothesis that early inflammatory and oxidative mechanisms are already engaged. These processes are known to involve phospholipases A₂ and L-amino acid oxidases (LAAOs), leading to the generation of reactive oxygen species (ROS) and subsequent activation of cell-damage signaling pathways (Naumann et al., 2011).

Finally, the vascular congestion detected in both experimental groups likely represents an early hepatic response to envenomation. This is consistent with the findings of Sarkar et al. (2021), who emphasized hepatotoxicity as a key effect of snake venom, attributable to the central role of the liver in toxin metabolism and neutralization. Collectively, these data reinforce the liver's vulnerability to early venom-induced alterations, which may progress to more severe injury over time.

Histopathological and quantitative analyses demonstrated overall preservation of splenic architecture across all experimental groups (PBS, BmPLA₂-A, and *Bothrops mattogrossensis* venom). The distinction between white and red pulp compartments remained well defined, with homogeneous lymphoid aggregates in the white pulp and erythrocyte-rich sinusoids in the red pulp. Quantitatively, nuclear area and structural coherence remained comparable among groups, indicating preserved cellular integrity and microarchitectural organization. The only statistically significant alteration was an increase in vascular congestion in the *BmV* group, corroborating the morphological evidence of enhanced sinusoidal dilation and erythrocyte accumulation within the red pulp.

These findings suggest that *B. mattogrossensis* venom induces early but mild splenic vascular responses without compromising the overall parenchymal organization. The observed vascular congestion likely reflects transient hemodynamic changes rather than structural damage, consistent with an early stage of systemic venom activity.

Previous studies have shown that snake venoms can induce hematological and vascular disturbances, including severe coagulopathies such as venom-induced consumption coagulopathy (VICC), often leading to systemic or organ-specific hemorrhage, including in the spleen (Kasturiratne et al., 2021; Otieno et al., 2021; Wedasingha et al., 2020). Venom components such as metalloproteinases, serine proteases, and phospholipases A₂ are known to increase vascular permeability and promote hemorrhage (Silva et al., 2022; Senthilkumaran et al., 2021). However, in the present study, neither BmPLA₂-A nor crude venom produced such outcomes, suggesting that the administered dose and the short post-exposure interval were insufficient to elicit substantial endothelial disruption or splenic hemorrhage.

Although splenic hemorrhage has occasionally been reported in severe envenomation cases, it is typically associated with extensive coagulopathy, where synergistic venom activities result in consumption of coagulation factors and widespread vascular injury (Senthilkumaran et al., 2021; Anjana-Silva et al., 2022; Lee and Sung, 2019). The structural preservation observed here therefore likely reflects an early, pre-hemorrhagic stage of toxin exposure, in which congestion represents a reversible microvascular event preceding overt tissue injury.

These findings also emphasize the importance of temporal context and dosing in assessing venom-induced effects in different organs. Clinical studies highlight that early administration of antivenom and adequate hemodynamic support are critical to prevent severe complications, including splenic hemorrhage (Maduwage and Isbister, 2014; Cinquantini et al., 2018; Chen et al., 2023). Collectively, the present results suggest that, during the early stages of envenomation, splenic histological changes may be minimal, particularly in controlled experimental models.

The hemorrhagic activity of *B. mattogrossensis* venom and the BmPLA₂-A in the gastrocnemius muscle was assessed by measuring hemorrhagic halo formation and hemoglobin levels. The results corroborate previous findings and the histological analyses of this study. While the venom exhibited marked hemorrhagic activity, BmPLA₂-A did not induce this effect, reinforcing that PLA₂s are not the main hemorrhagic agents in *Bothrops* venoms. This observation aligns with studies emphasizing the central role of zinc-dependent metalloproteinases (SVMPs) in hemorrhage induction. For instance, Nina-Cueva et al. (2020) demonstrated that the venoms of *Bothrops roedingeri* and *Bothrops brazili* display SVMP-mediated hemorrhagic activity, involving P-I and P-III classes that degrade extracellular matrix components and disrupt endothelial integrity. Similarly, Gay et al. (2013) highlighted the importance of SVMPs, such as baltergin, in mediating local hemorrhage in *Bothrops alternatus* venom.

Regarding myotoxicity, serum CK levels were significantly elevated in mice inoculated with *B. mattogrossensis* venom but not in those inoculated with BmPLA₂-A, suggesting that SVMPs contribute more prominently to muscle damage. This finding is consistent with reports of synergism between PLA₂s and SVMPs in inducing myotoxicity. Bustillo et al. (2012) demonstrated that the combination of baltergin (SVMP) and Ba SpII RP4 (PLA₂) exerted a synergistic cytotoxic effect on myoblast cultures. The absence of significant CK elevation following BmPLA₂-A treatment suggests limited myotoxic potential when isolated, although it still contributes to local inflammation and tissue damage, as evidenced by increased IL-1β in muscle tissue.

The elevated CK levels observed after crude *B. mattogrossensis* venom administration are consistent with the characteristic myotoxicity of *Bothrops* venoms, typically mediated by both PLA₂s and SVMPs. Gay et al. (2013) reported that *B. diporus* venom induced a greater CK increase than *B. alternatus* venom, reflecting its higher content of myotoxic PLA₂s. However, the lack of CK elevation with BmPLA₂-A contrasts with studies describing highly myotoxic PLA₂s, such as BaTX from *B. alternatus*, which induced rapid and pronounced CK release (Ponce-Soto et al., 2007). This discrepancy may be related to structural

and functional variations among PLA₂s, which affect their affinity for cell membranes and myotoxic potential (Lomonte and Krizaj, 2021).

In summary, *B. mattogrossensis* venom and BmPLA₂-A induce systemic effects through distinct mechanisms. Snake venom likely acts through synergistic interactions between SVMPs and PLA₂s, leading to vascular injury and widespread organ dysfunction, whereas BmPLA₂-A exerts a more localized effect in muscle tissue. Nonetheless, the occurrence of pathological alterations in multiple organs in both groups indicates that the effects are not confined to the injection site, highlighting the complexity of *Bothrops* venom action and the need for further studies to elucidate the interactions between isolated toxins and the venom.

The comparative analysis of *B. mattogrossensis* venom and isolated BmPLA₂-A highlights the complexity of envenomation pathology. Whole venom induced widespread tissue injury, most notably skeletal muscle necrosis, pulmonary and renal alterations, hepatic stress, and pronounced hemorrhage, consistent with the combined action of SVMPs, PLA₂ isoforms, and other toxins. In contrast, BmPLA₂-A displayed minimal pathological effects, indicating either low intrinsic toxicity or a requirement for synergistic interactions with other venom components to elicit damage.

These findings illustrate the principle of toxin synergy in snake venoms, where the concerted action of multiple enzymatic families produces the full spectrum of pathological effects observed clinically. The absence of significant effects with isolated BmPLA₂-A highlights the importance of metalloproteinases in driving vascular, renal, hepatic, and hemorrhagic damage, while also suggesting that not all PLA₂s within *Bothrops* venoms are potent myotoxins.

Overall, this study demonstrates that *B. mattogrossensis* venom exerts multisystem pathological effects, including severe skeletal muscle necrosis, systemic hemorrhage, pulmonary and renal alterations, and hepatic stress. In contrast, BmPLA₂-A induced only discrete changes, insufficient to elicit measurable hemorrhagic or myotoxic outcomes under the conditions tested, indicating that this molecule displays a markedly attenuated toxic phenotype relative to the whole venom.

Through a clinical and translational perspective, these data underscore two complementary implications. First, they reinforce the need for polyvalent antivenoms that neutralize diverse toxin families responsible for the complex pathology of *Bothrops* envenomation. Second, and importantly for biotechnology and drug discovery, the identification of a catalytically active yet non-myotoxic PLA₂ such as BmPLA₂-A highlights a class of venom proteins that can be repurposed or engineered for therapeutic and investigative use. Snake-venom PLA₂s have been repeatedly recognized as both targets for small-molecule inhibition and as molecular scaffolds with direct biomedical applications: small-molecule PLA₂ inhibitors (for example, varespladib and its prodrug varespladib-methyl) have been developed to neutralize secreted PLA₂ activity in envenomation and are currently under clinical evaluation as broad-spectrum adjuncts to antivenom therapy, illustrating the translational tractability of targeting venom PLA₂s (Lewin et al., 2022; Oliveira et al., 2022).

Beyond antivenom strategies, several lines of published work indicate diverse pharmacological opportunities for PLA₂-derived molecules or PLA₂-inspired derivatives. First, because PLA₂s control the release of arachidonic acid and lysophospholipids, key precursors of eicosanoids and bioactive lysophospholipids, catalytically competent but non-toxic PLA₂s can be used as precise biochemical tools to probe lipid signaling pathways, membrane remodeling, and ferroptosis-related processes in cell and tissue models. Such uses facilitate mechanistic studies of inflammation and lipid-mediated cell death that are relevant to inflammatory diseases and cancer (Calderon et al., 2014).

Second, venom PLA₂s and PLA₂-derived peptides have been explored as scaffolds for novel therapeutics with anti-inflammatory, antimicrobial and anticancer activities. Multiple preclinical studies and reviews report that sequence-guided truncation or chemical modification of svPLA₂s yields peptides with selective cytotoxicity against tumor cells, antimicrobial activity against pathogens, or modulatory effects on immune signaling, properties that make them attractive leads for medicinal chemistry optimization and peptidomimetic design. These efforts are complemented by structure, function studies that map active and surface regions amenable to mutation or grafting, enabling the generation of non-toxic variants with retained beneficial bioactivities (Sun et al., 2021).

Collectively, our findings position BmPLA₂-A as a catalytically active (Eulálio et al., 2025) yet non-myotoxic PLA₂ that not only enhances understanding of *B. mattogrossensis* venom pathology but also represents a promising lead for biotechnological exploration, including structure–function mapping, lipidomic profiling, and early-stage medicinal chemistry aimed at generating safe and effective PLA₂-inspired bioactive molecules.

5. Conclusion

This study demonstrates that *Bothrops mattogrossensis* venom exerts profound multisystem toxicity characterized by skeletal muscle necrosis, pulmonary and renal vascular injury, hepatic stress, and potent hemorrhagic activity, effects that are absent or minimal when the BmPLA₂-A is administered in isolation. These findings underscore the principle of toxin synergy, whereby PLA₂, metalloproteinases, and other venom constituents interact to amplify tissue damage and systemic pathology. Clinically, these insights reinforce the necessity of antivenoms with broad neutralizing capacity against multiple toxin families. From a translational perspective, the identification of catalytically active yet non-myotoxic PLA₂s such as BmPLA₂-A opens avenues for pharmacological exploration, providing potential molecular tools for probing lipid signaling and therapeutic innovation.

Funding

The authors express their gratitude to Conselho Nacional de Desenvolvimento Científico e Tecnologico (CNPq), Coordenação de Aperfeiçoamento de Pessoal de Nível Superior (CAPES), and Fundação de Amparo à Pesquisa do Estado de Rondônia (FAPERO) for the financial support. The authors thank the Network Technological Platforms from FIOCRUZ for the support and financing of the services provided by Microscopy (RPT-7I), and Bioprospecting and Molecular Interaction (RPT-10B) facilities/FIOCRUZ-Rondonia. This study was supported by grants (428774/2016–4 and 311696/2021–0) from Conselho Nacional de Desenvolvimento Científico e Tecnológico (CNPq). Juliana Pavan Zuliani was a recipient of a productivity grant 311696/2021–0 from Conselho Nacional de Desenvolvimento Científico e Tecnológico (CNPq) and Micaela de Melo Cordeiro Eulálio benefited from a Doctoral fellowship provided by CAPES.

CRediT authorship contribution statement

Micaela de Melo Cordeiro Eulálio: Conceptualization, Investigation, Methodology, Writing – original draft. **Cindy de Oliveira Bariani:** Methodology, Writing – original draft. **Alex Augusto Ferreira e Ferreira:** Data curation, Formal analysis, Methodology, Writing – original draft. **Andréia Nalva Bernardi de Lima:** Formal analysis, Methodology. **Hallison Mota Santana:** Formal analysis, Methodology. **Mauro Valentino Paloschi:** Formal analysis, Methodology. **Sulamita da Silva Setúbal:** Formal analysis, Methodology. **Larissa Faustina Cruz:** Formal analysis, Methodology. **Ketlei Monteiro Tavares:** Formal analysis, Methodology. **Carolina Pereira da Silva:** Formal analysis, Methodology. **Milena Daniela Souza Silva:** Formal analysis, Methodology. **Charles Nunes Boeno:** Formal analysis, Methodology. **Paula Helena Santa Rita:** Methodology, Resources. **Andreimar Martins Soares:** Methodology, Resources. **Daniela Priscila Marchi Salvador:** Methodology, Resources. **Juliana Pavan Zuliani:** Conceptualization, Data curation, Formal analysis, Funding acquisition, Project administration, Writing – original draft, Writing – review & editing.

Declaration of competing interest

The authors declare that they have no known competing financial interests or personal relationships that could have appeared to influence the work reported in this paper.

Data availability

Data will be made available on request.

References

Alangode, A., Rajan, K., Nair, B.G., 2020. Snake antivenom: challenges and alternate approaches. Biochem. Pharmacol. 181. https://doi.org/10.1016/j.bcp.2020.114135.

Amaral, C.F., de Rezende, N.A., da Silva, O.A., Ribeiro, M.M., Magalhães, R.A., dos Reis, R.J., Carneiro, J.G., Castro, J.R., 1986. Acute kidney failure secondary to ophidian bothropic and crotalid accidents: analysis of 63 cases. Rev. Inst. Med. Trop. 28, 220–227.

Angulo, Y., Lomonte, B., 2009. Biochemistry and toxicology of toxins purified from the venom of the snake *Bothrops asper*. Toxicon 54, 949–957. https://doi.org/10.1016/j.toxicon.2008.12.014.

Ángel-Camilo, K.L., Bueno-Ospina, M.L., Bolaños Burgos, I.C., Ayerbe-González, S., Beltrán-Vidal, J., Acosta, A., Álvarez-Soler, J., Guerrero-Vargas, J.A., 2024. Cardiotoxic effects of *Lachesis acrochorda* snake venom in anesthetized Wistar rats. Toxins (Basel) 16, 377. https://doi.org/10.3390/toxins16090377.

Anjana-Silva, Scorgie, F.E., Lincz, L.F., Maduwage, K., Siribaddana, S., Isbister, G.K., 2022. Indian polyvalent antivenom accelerates recovery from venom-induced consumption coagulopathy (VICC) in Sri Lankan Russell's viper (*Daboia russelii*) envenoming. Front. Med. (Lausanne) 9, 852651. https://doi.org/10.3389/fmed.2022.852651.

Asega, A.F., Menezes, M.C., Trevisan-Silva, D., Cajado-Carvalho, D., Bertholim, L., Oliveira, A.K., et al., 2020. Cleavage of proteoglycans, plasma proteins and the platelet-derived growth factor receptor in the hemorrhagic process induced by snake venom metalloproteinases. Sci. Rep. 10, 12912. https://doi.org/10.1038/s41598-020-69396-y.

Baldo, C., Jamora, C., Yamanouye, N., Zorn, T.M., Moura-da-Silva, A.M., 2010. Mechanisms of vascular damage by hemorrhagic snake venom metalloproteinases: tissue distribution and in situ hydrolysis. PLoS Negl. Trop. Dis. 4, e727. https://doi.org/10.1371/journal.pntd.0000727.

Barraviera, B., Pereira, P.C.M., 1995. Accidents Caused By Snakes of the Genus *Bothrops. Venenos animais: Uma Visão Integrada*. de Publicações Científicas, Rio de Janeiro, pp. 261–280.

Bustillo, S., Gay, C.C., García Denegri, M.E., Ponce-Soto, L.A., Bal de Kier Joffé, E., Acosta, O., Leiva, L.C., 2012. Synergism between baltergin metalloproteinase and Ba SPII RP4 PLA_2 from *Bothrops alternatus* venom on skeletal muscle (C2C12) cells. Toxicon 59, 338–343.

Calderon, L.A., Sobrinho, J.C., Zaqueo, K.D., de Moura, A.A., Grabner, A.N., Mazzi, M.V., Marcussi, S., Nomizo, A., Fernandes, C.F., Zuliani, J.P., Carvalho, B.M., da Silva, S.L., Stábeli, R.G., Soares, A.M., 2014. Antitumoral activity of snake venom proteins: new trends in cancer therapy. Biomed. Res. Int. 2014, 203639. https://doi.org/10.1155/2014/203639.

Campbell, J.A., Lamar, W.W., 2004. The Venomous Reptiles of the Western Hemisphere. Comstock Publishing Associates, Ithaca, NY.

Chen, H., Unberath, M., Dreizin, D., 2023. Toward automated interpretable AAST grading for blunt splenic injury. Emerg. Radiol. 30, 41–50. https://doi.org/10.1007/s10140-022-02099-1.

Cinquantini, F., Simonini, E., Di Saverio, S., et al., 2018. Non-surgical management of blunt splenic trauma: a comparative analysis of non-operative management and splenic artery embolization - experience from a European trauma center. Cardiovasc. Intervent. Radiol. 41, 1324–1332. https://doi.org/10.1007/s00270-018-1953-9.

Eulálio, M.M.C., de Lima, A.M., Brant, R.S.C., Francisco, A.F., Santana, H.M., Paloschi, M.V., Setúbal, S.S., da Silva, C.P., Silva, M.D.S., Boeno, C.N., Kayano, A.M., Rita, P.H.S., Calderon, L.A., Soares, A.M., Salvador, D.P.M., Zuliani, J.P., 2025. Characterization of a novel acidic phospholipase A_2 isolated from the venom of *Bothrops mattogrossensis*: from purification to structural modeling. Int. J. Biol. Macromol. 292, 139217. https://doi.org/10.1016/j.ijbiomac.2024.139217.

Gay, C., Maruñak, S., Teibler, P., Leiva, L., Acosta, O., 2013. Effect of monospecific antibodies against baltergin in myotoxicity induced by *Bothrops alternatus* venom from northeast Argentina: role of metalloproteinases in muscle damage. Toxicon 63, 104–111. https://doi.org/10.1016/j.toxicon.2012.11.028.

Gutiérrez, J.M., Escalante, T., Rucavado, A., Herrera, C., 2016. Hemorrhage caused by snake venom metalloproteinases: a journey of discovery and understanding. Toxins (Basel) 8, 93. https://doi.org/10.3390/toxins8040093.

Kasturiratne, A., Lalloo, D.G., de Silva, H.J., 2021. Chronic health effects and cost of snakebite. Toxicon X 9–10, 100074. https://doi.org/10.1016/j.toxcx.2021.100074.

Khan, S.A., Ilies, M.A., 2023. The phospholipase A_2 superfamily: structure, isozymes, catalysis, physiologic and pathologic roles. Int. J. Mol. Sci. 24, 1353. https://doi.org/10.3390/ijms24021353.

Khimmaktong, W., Nuanyaem, N., Lorthong, N., Hodgson, W.C., Chaisakul, J., 2022. Histopathological changes in the liver, heart and kidneys following Malayan pit viper (*Calloselasma rhodostoma*) envenoming and the neutralising effects of hemato polyvalent snake antivenom. Toxins (Basel) 14, 601. https://doi.org/10.3390/toxins14090601.

Lee, H.S., Sung, W.Y., 2019. A case of non-operative management of atraumatic splenic hemorrhage due to snakebite venom-induced consumption coagulopathy. Am. J. Case Rep. 20, 1314–1319. https://doi.org/10.12659/AJCR.918040.

Lewin, M.R., Carter, R.W., Matteo, I.A., Samuel, S.P., Rao, S., Fry, B.G., Bickler, P.E., 2022. Varespladib in the treatment of snakebite envenoming: development history and preclinical evidence supporting advancement to clinical trials. Toxins (Basel) 14, 783. https://doi.org/10.3390/toxins14110783.

Lomonte, B., Križaj, I., 2021. Snake venom phospholipase A_2 toxins. In: Mackessy, S.P. (Ed.), Handbook of Venoms and Toxins of Reptiles, 2nd ed. CRC Press, Boca Raton.

Mackessy, S.P., 2021. Handbook of Venoms and Toxins of Reptiles, 2nd ed. CRC Press, Boca Raton. https://doi.org/10.1201/9780429054204.

Madrigal, M., Sanz, L., Flores-Díaz, M., Sasa, M., Núñez, V., Alape-Girón, A., Calvete, J.J., 2012. Snake venomics across genus *Lachesis*: ontogenetic changes in *Lachesis stenophrys* and comparative proteomics of venoms of adult *Lachesis melanocephala* and *Lachesis acrochorda*. J. Proteom. 77, 280–297. https://doi.org/10.1016/j.jprot.2012.09.003.

Maduwage, K., Isbister, G.K., 2014. Current treatment for venom-induced consumption coagulopathy resulting from snakebite. PLoS Negl. Trop. Dis. 8, e3220. https://doi.org/10.1371/journal.pntd.0003220.

Mamede, C.C.N., de Sousa Simamoto, B.B., da Cunha Pereira, D.F., de Oliveira Costa, J., Ribeiro, M.S.M., de Oliveira, F., 2020. Edema, hyperalgesia and myonecrosis induced by Brazilian *Bothrops* venoms: an overview of the last decade. Toxicon 187, 10–18. https://doi.org/10.1016/j.toxicon.2020.08.016.

Marinho, A.D., Silveira, J.A.M., Chaves Filho, A.J.M., Jorge, A.R.C., Nogueira Júnior, J., Pereira, V.B.M., de Aquino, P.E.A., Pereira, C.A.S., Evangelista, J.S.A.M., Macedo, D. S., Lima Júnior, R.C.P., Toyama, M.H., Jorge, R.J.B., Pereira, G.J.S., Monteiro, H.S. A., 2021. *Bothrops pauloensis* snake venom–derived Asp-49 and Lys-49 phospholipases A_2 mediate acute kidney injury by oxidative stress and release of inflammatory cytokines. Toxicon 190, 31–38. https://doi.org/10.1016/j.toxicon.2020.12.004.

Mello, S.M., Linardi, A., Rennó, A.L., Tarsitano, C.A., Pereira, E.M., Hyslop, S., 2010. Renal kinetics of *Bothrops alternatus* (Urutu) snake venom in rats. Toxicon 55, 470–480.

Meena, P., Bhargava, V., Gupta, P., et al., 2024. The renal histopathological spectrum in patients with kidney injury following snakebite envenomation in India: a five-decade scoping review. BMC Nephrol 25, 112. https://doi.org/10.1186/s12882-024-03508-y.

Mittal, B.V., 1994. Acute renal failure following poisonous snake bite. J. Postgrad. Med. 40, 123–126.

Naumann, G.B., Silva, L.F., Silva, L., Faria, G., Richardson, M., Evangelista, K., Kohlhoff, M., Gontijo, C.M., Navdaev, A., de Rezende, F.F., Eble, J.A., Sanchez, E.F., 2011. Cytotoxicity and inhibition of platelet aggregation caused by an L-amino acid oxidase from *Bothrops leucurus* venom. Biochim. Biophys. Acta 1810, 683–694. https://doi.org/10.1016/j.bbagen.2011.04.003.

Nina-Cueva, O., Olazabal-Chambilla, D., Quispe-Arpasi, J., Alzamora-Sánchez, A., Gomes-Heleno, M., Huancahuire-Vega, S., 2020. Biochemical characterization of *Bothrops roedingeri* Mertens, 1942 snake venom and its edematogenic, hemorrhagic, and myotoxic activities. Biomedica 40, 682–692. https://doi.org/10.7705/biomedica.5228.

Nonaka, P.N., Amorim, C.F., Paneque Peres, A.C., E Silva, C.A., Zamuner, S.R., Ribeiro, W., Cogo, J.C., Vieira, R.P., Dolhnikoff, M., de Oliveira, L.V., 2008. Pulmonary mechanics and lung histology injury induced by *Crotalus durissus terrificus* snake venom. Toxicon 51, 1158–1166. https://doi.org/10.1016/j.toxicon.2008.02.006.

Oliveira Neto, J., Silveira, J.A.M., Serra, D.S., Viana, D.A., Borges-Nojosa, D.M., Sampaio, C.M.S., Monteiro, H.S.A., Cavalcante, F.S.Á., Evangelista, J.S.A.M., 2017. Pulmonary mechanics and lung histology induced by *Crotalus durissus cascavella* snake venom. Toxicon 137, 144–149. https://doi.org/10.1016/j.toxicon.2017.07.023.

Oliveira, A.L., Viegas, M.F., da Silva, S.L., 2022. The chemistry of snake venom and its medicinal potential. Nat. Rev. Chem. 6, 451–469. https://doi.org/10.1038/s41570-022-00393-7.

Otero-Patiño, R., 2009. Epidemiological, clinical and therapeutic aspects of Bothrops asper bites. Toxicon 54, 998–1011.

Otieno, S.B., Wellikoff, S.K., Weir, A., Ogbeide, O., 2021. Managing massive splenic hematoma: exploratory laparotomy or active surveillance? Cureus 13, e14967. https://doi.org/10.7759/cureus.14967.

Ponce-Soto, L.A., Lomonte, B., Gutiérrez, J.M., Rodrigues-Simioni, L., Novello, J.C., Marangoni, S., 2007. Structural and functional properties of BaTX, a new Lys49 phospholipase A_2 homologue isolated from the venom of the snake *Bothrops alternatus*. Biochim. Biophys. Acta 1770, 585–593. https://doi.org/10.1016/j.bbagen.2006.11.015.

Pourakpour, F., Szölgyén, Á., Nateghi, R., Gutman, D.A., Manthey, D., Cooper, L.A.D., 2025. HistomicsTK: a Python toolkit for pathology image analysis algorithms. SoftwareX 31, 102318. https://doi.org/10.1016/j.softx.2025.102318.

Rodrigues, P.S.M., Martins, H.C., Falcão, M.S., Trevisan, M., Portaro, F.C.V., da Silva, L. G., Sano-Martins, I.S., Gonçalves, L.R.C., Seibert, C.S., 2023. Effects of *Mauritia flexuosa* L.f. (buriti) oil on symptoms induced by *Bothrops moojeni* snake envenomation. J. Ethnopharmacol. 313, 116612. https://doi.org/10.1016/j.jep.2023.116612.

Rodrigues Sgrignolli, L., Florido Mendes, G.E., Carlos, C.P., Burdmann, E.A., 2011. Acute kidney injury caused by *Bothrops* snake venom. Nephron Clin. Pract. 119, c131–c137. https://doi.org/10.1159/000324228.

Rucavado, A., Escalante, T., Teixeira, C.F., Fernándes, C.M., Díaz, C., Gutiérrez, J.M., 2002. Increments in cytokines and matrix metalloproteinases in skeletal muscle after injection of tissue-damaging toxins from the venom of the snake *Bothrops asper*. Mediators Inflamm 11, 121–128. https://doi.org/10.1080/09629350220131980.

Sampat, G.H., Hiremath, K., Dodakallanavar, J., Patil, V.S., Harish, D.R., Biradar, P., Mahadevamurthy, R.K., Barvaliya, M., Roy, S., 2023. Unraveling snake venom phospholipase A_2: an overview of its structure, pharmacology, and inhibitors. Pharmacol. Rep. 75, 1454–1473. https://doi.org/10.1007/s43440-023-00543-8.

Sano-Martins, I.S., Santoro, M.L., Castro, S.C., Fan, H.W., Cardoso, J.L., Theakston, R.D., 1997. Platelet aggregation in patients bitten by the Brazilian snake *Bothrops jararaca*. Thromb. Res. 87, 183–195. https://doi.org/10.1016/S0049-3848(97)00118-7.

Sarkar, S., Sinha, R., Chaudhury, A.R., Maduwage, K., Abeyagunawardena, A., Bose, N., Pradhan, S., Bresolin, N.L., Garcia, B.A., McCulloch, M., 2021. Snakebite associated with acute kidney injury. Pediatr. Nephrol. 36, 3829–3840. https://doi.org/10.1007/s00467-020-04911-x.

Senthilkumaran, S., Vijayakumar, P., Savania, R., et al., 2021. Splenic rupture and subsequent splenectomy in a young healthy victim following Russell's viper bite. Toxicon 204, 9–13. https://doi.org/10.1016/j.toxicon.2021.10.010.

Silva, A., Isbister, G.K., 2020. Current research into snake antivenoms, their mechanisms of action and applications. Biochem. Soc. Trans. 48, 537–546. https://doi.org/10.1042/BST20190739.

Silva, M.D.S., Lopes, J.A., Paloschi, M.V., Boeno, C.N., Rego, C.M.A., de Oliveira Sousa, O., Santana, H.M., dos Reis, V.P., Serrath, S.N., da Setúbal, S.S., Lima, A.M., Soares, A.M., Zuliani, J.P., 2022. NLRP3 inflammasome activation in human peripheral blood mononuclear cells induced by venoms' secreted PLA_2s. Int. J. Biol. Macromol. 202, 597–607. https://doi.org/10.1016/j.ijbiomac.2022.01.107.

Sitprija, V., Sitprija, S., 2012. Renal effects of snake venom toxins: pathophysiology and clinical implications. Nat. Rev. Nephrol. 8, 653–662. https://doi.org/10.1038/nrneph.2012.171.

Sun, G.Y., Geng, X., Teng, T., Yang, B., Appenteng, M.K., Greenlief, C.M., Lee, J.C., 2021. Dynamic role of phospholipases A_2 in health and diseases in the central nervous system. Cells 10, 2963. https://doi.org/10.3390/cells10112963.

Trevisan-Silva, D., Cosenza-Contreras, M., Oliveira, U.C., da Rós, N., Andrade-Silva, D., Menezes, M.C., Oliveira, A.K., Rosa, J.G., Sachetto, A.T.A., Biniossek, M.L., Pinter, N., Santoro, M.L., Nishiyama-Jr, M.Y., Schilling, O., Serrano, S.M.T., 2023. Systemic toxicity of snake venom metalloproteinases: multi-omics analyses of kidney and blood plasma disturbances in a mouse model. Int. J. Biol. Macromol. 253, 127279. https://doi.org/10.1016/j.ijbiomac.2023.127279.

Triggiani, M., Granata, F., Frattini, A., Marone, G., 2006. Activation of human inflammatory cells by secreted phospholipases A_2. Biochim. Biophys. Acta 1761, 1289–1300. https://doi.org/10.1016/j.bbalip.2006.07.003.

Wedasingha, S., Isbister, G., Silva, A., 2020. Bedside coagulation tests in diagnosing venom-induced consumption coagulopathy in snakebite. Toxins (Basel) 12, 583. https://doi.org/10.3390/toxins12090583.

World Health Organization, 2019. Snakebite envenoming: WHO Strategy For Prevention and Control. World Health Organization, Switzerland. https://coilink.org/20.500.12592/282cnm (accessed 22 Jul. 2025)COI: 20.500.12592/282cnm.

Zuliani, J.P., Souza, R.D., Setúbal, S.S., Boeno, C.N., Lopes, J.A., Zamuner, S.R., 2023. Inflammatory effects of phospholipase A_2s present in snake venom of the genus *Bothrops*. In: Chakraborti, S. (Ed.), Phospholipases in Physiology and Pathology, Phospholipases in Physiology and Pathology, 4. Academic Press, Elsevier, pp. 173–196.